The Hall dynamo effect and nonlinear mode coupling during sawtooth magnetic reconnection

W. X. Ding,[1,2] D. L. Brower,[1,2] B. H. Deng,[1] A. F. Almagri,[2,3] D. Craig,[2,3] G. Fiksel,[2,3]
V. Mirnov,[2,3] S. C. Prager,[2,3] J. S. Sarff,[2,3] and V. Svidzinski[2,3]

[1]*Electrical Engineering Department, University of California at Los Angeles, Los Angeles, California 90095*
[2]*Center for Magnetic Self-Organization in Laboratory and Astrophysical Plasmas, University of Wisconsin-Madison, Madison, Wisconsin 53706*
[3]*Department of Physics, University of Wisconsin-Madison, Madison, Wisconsin 53706*

During magnetic reconnection associated with sawtooth activity in a reversed field pinch, we observe a large fluctuation-induced Hall electromotive force, $\langle \delta \mathbf{J} \times \delta \mathbf{B} \rangle / n_e e$, which is capable of modifying the equilibrium current. This Hall dynamo effect is determined in the hot plasma core by laser Faraday rotation which measures equilibrium and fluctuating magnetic field and current density. We find that the Hall dynamo is strongest when nonlinear mode coupling between three spatial Fourier modes of the resistive tearing instability is present. Mode coupling alters the phase relation between magnetic and current density fluctuations for individual Fourier modes leading to a finite Hall effect. Detailed measurements of the spatial and temporal dynamics for the dominant core resonant mode under various plasma configurations are described providing evidence regarding the origin of the Hall dynamo. © *2006 American Institute of Physics*. [DOI: 10.1063/1.2363353]

I. INTRODUCTION

Magnetic reconnection is an important process in both laboratory and naturally occurring magnetized plasmas. Perhaps the best known example for laboratory plasmas is the tokamak sawtooth cycle for the $m=n=1$ tearing mode,[1] where m and n are the poloidal and toroidal mode numbers, respectively. A process that resembles this sawtooth cycle also occurs in some reversed field pinch (RFP) plasmas. In the RFP, the sawtooth cycle is connected to the magnetic dynamo, or self-generation of mean current and magnetic flux, well known to underlie the self-organization of RFP and spheromak plasmas. A standard model for the RFP dynamo is provided by nonlinear resistive magnetohydrodynamic (MHD) theory.[2] A portion of this model has been experimentally confirmed, but the measurements are incomplete, due to the complexity of correlating three dimensional fluctuations of difficult to measure quantities.

Magnetic reconnection is governed by the generalized Ohm's law, i.e., the electron momentum equation[3]

$$-\frac{m_e}{e^2 n_e}\frac{\partial \mathbf{J}}{\partial t} + \mathbf{E} + \mathbf{v} \times \mathbf{B} - \frac{1}{n_e e}\mathbf{J} \times \mathbf{B} + \frac{\nabla P_e}{n_e e} = \eta \mathbf{J}, \quad (1a)$$

where n_e and m_e are the electron density and mass, e is the electron charge, and P_e is the electron pressure. J, E, v, B, and η are the plasma current density, electric field, ion velocity, magnetic field, and resistivity, respectively. This equation can be written in the general form[4]

$$\mathbf{E} + \mathbf{v} \times \mathbf{B} = \mathbf{R}, \quad (1b)$$

where $\mathbf{R}$ is any nonideal term due to collisions, particle inertia, diamagnetic effects, or any fluctuation-induced force. Some nonideal effects violate the frozen plasma condition and cause breaking of magnetic field lines leading to reconnection. Electric field E is a measure of the change of mag-

netic flux and therefore is sometimes referred to as the reconnection rate.[5] Determination of the electric field and nonideal effects are critical elements required to understand magnetic reconnection physics.

Possible dynamo mechanisms originate from generalized Ohm's law by considering spatial (and possibly temporal) fluctuations in the various fields contained in the two-fluid description. The parallel mean-field Ohm's law can be constructed to isolate these dynamo mechanisms by decomposing each variable quantity in Eq. (1a) into mean and fluctuating parts. Taking the ensemble average of the component along the mean magnetic field direction yields

$$\langle E_\parallel \rangle + \langle \delta \mathbf{v} \times \delta \mathbf{B} \rangle_\parallel - \langle \delta \mathbf{J} \times \delta \mathbf{B} \rangle_\parallel / n_e e = \eta_\parallel \langle J_\parallel \rangle, \quad (2)$$

where δ denotes a fluctuating quantity and $\langle \ \rangle$ denotes a mean or ensemble-averaged quantity. The inertial term (dJ/dt) is negligible in the experiments described here, and all quadratic terms driven by density and electron pressure fluctuations vanish upon ensemble averaging. We note that mean current (the right hand side) can be generated by two fluctuation-induced terms: the MHD dynamo (second term on the left-hand side) arising from the correlation of magnetic and flow velocity fluctuations, and the Hall dynamo (third term on the left-hand side) arising from the coherent interaction of magnetic and current density fluctuations.

It is well established experimentally that $\langle E \rangle_\parallel \neq \eta_\parallel \langle J \rangle_\parallel$ in RFP plasmas sustained at constant current and flux. To date, the majority of theoretical and experimental investigation of the balancing of Ohm's law has focused on the MHD dynamo. It is also noteworthy that a simple Ohm's law is also not satisfied in sawtoothing tokamak plasmas in the vicinity of the $m=n=1$ resonant surface. Wesson[1,6] observed that the electric field generated by the reconnected helical flux near the $m=n=1$ resonant layer is so large that simple resistive

dissipation is inadequate to describe Joint European Torus (JET) tokamak plasmas. He suggests that large electron inertia is able to account for the imbalance between the electric field and current in Ohm's law. Another model suggests that stochastization of field lines, resulting from the interaction of fundamental $m=n=1$ helical mode with modes of other periodicities, plays an important role in the sawtooth collapse.[7] The possibility for dynamo effects has not been investigated.

In this paper we consider the dynamo process as observed in Madison Symmetric Torus (MST) RFP plasmas.[8] In MST, the sawtooth cycle is very distinct and robust, providing a convenient marker for diagnosing magnetic relaxation effects. (Plasmas in other RFP experiments exhibit less robust sawtooth behavior for unknown reasons.) In the sawtooth crash phase, magnetic flux generation is particularly strong, and there is a fast global change in the equilibrium current profile. There are other connected effects as well, such as a degradation in energy and particle confinement, which are not discussed here. Multiple tearing instabilities are observed throughout the sawtooth cycle, attaining their largest amplitude just before or during the crash. In the nonlinear resistive MHD model,[9] these tearing modes create a $\langle \delta \mathbf{v} \times \delta \mathbf{B} \rangle$ dynamo which balances Ohm's law. Probe measurements in the low-temperature plasma edge[10] ($r/a > 0.90$) reveal that Ohm's law is indeed balanced by the $\langle \delta \mathbf{v} \times \delta \mathbf{B} \rangle$ (MHD) dynamo. It is interesting to note, however, that the MHD dynamo in these experiments disappears as the probes are moved toward the plasma interior ($r/a = 0.85$). It may be important that this is also the vicinity of the toroidal field reversal surface where $m=0$ modes are resonant. In the high-temperature plasma core ($r/a < 0.5$), measurements using passive Doppler spectrometry reveal significant MHD dynamo associated with $m=1$ modes, but the radial resolution was limited by the chord-integrating nature of the measurement.[11] Active spectroscopy is currently being developed to localize the core MHD dynamo measurements.

Recent analytical quasilinear calculations suggest that the Hall dynamo may be dominant for the hot plasma interior, at least near a mode-rational surface.[12] Calculations of Hall dynamo for astrophysical applications[13,14] and laboratory plasma measurements[15,16] also indicate that the Hall dynamo is significant. Therefore, experimental measurements of all important terms in the generalized Ohm's law with good radial resolution spanning the minor radius are necessary to understand a possible composite dynamo process that includes both MHD and Hall dynamo physics.

In this paper, a fast laser-based Faraday rotation diagnostic is employed to measure magnetic field and current density changes during reconnection events for sawtoothing plasmas in MST. Both the time evolution of the profiles of the mean (axisymmetric) quantities and the fluctuations of magnetic field and current density are measured. We report two experimental results. First, the two-fluid Hall dynamo effect is large and balances the mean inductive electric field produced during the sawtooth crash in the hot plasma core for the dominant core resonant mode. The current density profile (and its change during a sawtooth crash) is determined by a combination of the Hall dynamo and inductive electric field.

The Hall dynamo is generated by tearing instabilities, which are manifest as several spatial Fourier modes. Second, we observe that the Hall dynamo is strongest when nonlinear coupling between spatial Fourier modes is present. Nonlinear coupling alters the phase relationship between current and magnetic field fluctuations so as to increase substantially the strength of the Hall dynamo. The two-fluid Hall electromotive force acts to regulate the plasma electric field and impacts the magnetic reconnection process.

This paper is organized as follows: in Sec. II, the experimental technique and analysis methods are described; in Sec. III, detailed experimental measurements of magnetic fluctuations and Hall dynamo in the core plasma are presented; Sec. IV contains discussion of Hall dynamo relative to MHD dynamo and the role played by the Hall dynamo in magnetic reconnection; and Sec. V contains a summary of experimental results and conclusions.

II. EXPERIMENTAL TECHNIQUE AND MEASUREMENT METHOD

The MST RFP is a toroidal confinement device, like the tokamak, but with toroidal magnetic field comparable to poloidal magnetic field.[8] It has major radius $R_o = 1.5$ m, minor radius $a = 0.52$ m. All data presented in this paper are for deuterium plasmas with discharge current $I_p = 350–400$ kA, line-averaged electron density $\bar{n}_e \sim 1 \times 10^{19}$ m^{-3}, reversal parameter $F(=B_\phi(a)/\langle B_\phi \rangle) \sim -0.22$, and electron temperature $T_e \sim T_i \sim 300$ eV. RFP plasmas have $q < 1$ everywhere within the plasma cross section [where $q = (r/R)(B_\phi/B_\theta)$ is the safety factor] and are therefore susceptible to large amplitude magnetic fluctuations dominated by tearing instabilities.[2] We focus here on standard RFP plasmas without current profile control so that magnetic fluctuations are large ($\sim 1\%$). A set of 64 equally spaced magnetic coils (with poloidal and toroidal separation) is used to measure magnetic fluctuations at the plasma edge due to resistive tearing modes. The magnetic fluctuation amplitude for a specified mode number (m,n) is obtained by spatial Fourier transformation from the magnetic coil array signals ($\sim b_{m,n} e^{i(m\theta + n\varphi)}$). Herein, we focus primarily on the role of the dominant, core resonant, (1,6) resistive tearing mode with frequency in the range $\sim 15–20$ kHz.

The internal equilibrium poloidal magnetic field, magnetic field fluctuations, and current density fluctuations are measured by a fast (time response ~ 4 μs) Faraday rotation diagnostic[17,18] where 11 vertical chords (separation ~ 8 cm) simultaneously probe the plasma cross section. The diagnostic approach employs two distinct but collinear far-infrared (FIR) laser beams to probe the plasma. The nonperturbing probe beams are frequency offset and have counter-rotating circular polarizations. Because of plasma birefringence, each beam experiences a different value of refractive index upon propagation through the plasma. The difference in refractive index is related to the Faraday rotation angle Ψ, according to the relation

$$\Psi = \frac{2\pi}{\lambda} \int \frac{(n_R - n_L)}{2} dz = 2.62 \times 10^{-13} \lambda_0^2 \int n_e B_z dz$$

$$= c_F \int n_e B_z dz, \qquad (3)$$

where B_z is the component of the magnetic field parallel to the FIR beams, n_e is the electron density, λ_0 is the laser wavelength, $z^2 = r^2 - x^2$, x is the impact parameter of probe beam ($x = 0$ corresponds to vacuum vessel center), and r is minor radius, all in MKS units. Refractive indices for the right-hand and left-hand circularly polarized waves are denoted by n_R and n_L, respectively. A multichord interferometer provides electron density along the same sightlines as the Faraday rotation measurement with the measured phase Φ, being given by

$$\Phi = \frac{2\pi}{\lambda} \int \frac{n_R + n_L}{2} dz \approx 2.82 \times 10^{-15} \lambda_0 \int n_e \, dz$$

$$= c_I \int n_e \, dz. \qquad (4)$$

The FIR laser beams are at nominal wavelength $\lambda_0 = 432$ μm (694 GHz) and operated at a slight difference frequency of $\Delta\omega/2\pi \approx 750$ kHz. The 11 chord polarimetry and interferometry data are routinely sampled at 1 MHz with the different frequency being aliased down to ~ 250 kHz. This results in a 4 μs time response (nonaliased time response ~ 1 μs), which is sufficient to follow the equilibrium and fluctuation dynamics of interest. A digital phase comparator technique is employed to extract the phase information for both the polarimeter and interferometer.[19] Typical polarimeter system rms noise levels are 1 mrad ($\approx 0.05°$) at 20 kHz bandwidth. Combined Faraday rotation and interferometer measurements enable us to infer internal magnetic field structure and its fluctuations. The equilibrium toroidal current density distribution is obtained from the measured poloidal field through use of Ampère's law.

Inductive toroidal electric field in the core plasma, induced by the sawtooth collapse, can also be determined using Faraday's law and is given by

$$E_\phi(r) = \frac{V_L}{2\pi R} - \int_r^a \frac{\partial}{\partial t} B_\theta(r') dr', \qquad (5)$$

where V_L is the loop voltage measured at the plasma surface and the second term is obtained by measurement of equilibrium dynamics.[20] In the plasma core, magnetic field direction is largely in the toroidal direction; therefore, $E_\phi \approx E_\parallel$. The electrical resistivity has been measured to be $\eta \sim (2-4) \times 10^{-7}$ Ω m^{-1} in this region.[21]
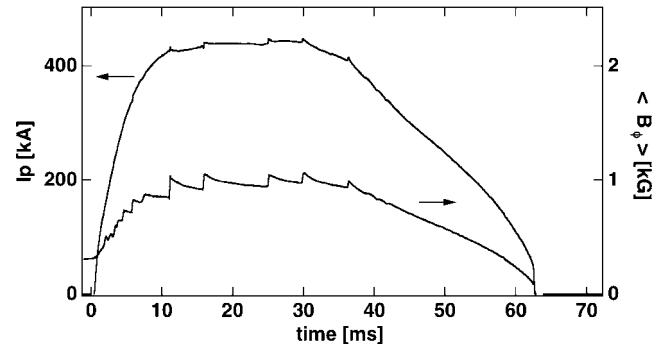

FIG. 1. Time history of plasma discharge current and toroidal magnetic field for a standard MST discharge. Each fast increase of toroidal magnetic field corresponds to a discrete sawtooth crash (or magnetic reconnection event).

For core magnetic and current density fluctuation measurements, detailed analysis of the phase signals is required. Since the measured Faraday rotation angle depends on both the density and magnetic field, it is necessary to separate the two in order to isolate the fluctuating magnetic field.[22] By rewriting Eq. (3) in terms of the equilibrium and fluctuating quantities for each variable (e.g., $\Psi = \Psi_0 + \tilde{\Psi}$, $B_z = B_{0z} + \tilde{B}_z$, $n_e = n_0 + \tilde{n}$), the fluctuating part of the Faraday rotation signal becomes

$$\tilde{\Psi} = c_F \left(\int B_{0z} \tilde{n} \, dz + \int \tilde{B}_z n_0 \, dz \right), \qquad (6)$$

where the second-order term, $c_F \int \tilde{B}_z \tilde{n} \, dz$, is negligible because both $\tilde{n}$ and $\tilde{B}_z$ are small. From this equation we see that the fluctuating part of the polarimetry signal is the sum of the fluctuating electron density weighted by equilibrium magnetic field, and the fluctuating magnetic field weighted by equilibrium density.

For the six chords nearest the magnetic axis, the $\int B_{0z} \tilde{n} \, dz$ term is negligible and $\tilde{\Psi} \approx c_F \int \tilde{B}_z n_0 \, dz$. This holds true for two reasons: (1) the component of the equilibrium poloidal field parallel to the central chords (B_{0z}) is small, and (2) $\int \tilde{n} \, dz \to 0$ for the measured fluctuations since $m = 1$.[23] By using measured values for equilibrium poloidal magnetic field and electron density fluctuations, it can be shown that $\int B_{0z} \tilde{n} \, dz \lesssim 0.05°$, which is less than the noise level. Finite contributions from the toroidal magnetic field to the Faraday signal resulting from misalignment have also been considered and found to be negligible. Further details on how the local magnetic and current density fluctuation information is obtained will be given in Sec. III C.

III. EXPERIMENTAL RESULTS

A. Equilibrium current density profile dynamics

Many parameters in MST plasmas display a sawtooth cycle due to relaxation oscillations in the plasma core. A typical MST discharge history is shown in Fig. 1. Sawtooth crashes, characterized by changes in toroidal flux, are denoted by prompt increases in the average toroidal field $\langle B_\phi \rangle$. To determine the time evolution of mean (magnetic surface averaged) quantities, we ensemble average measured quanti-
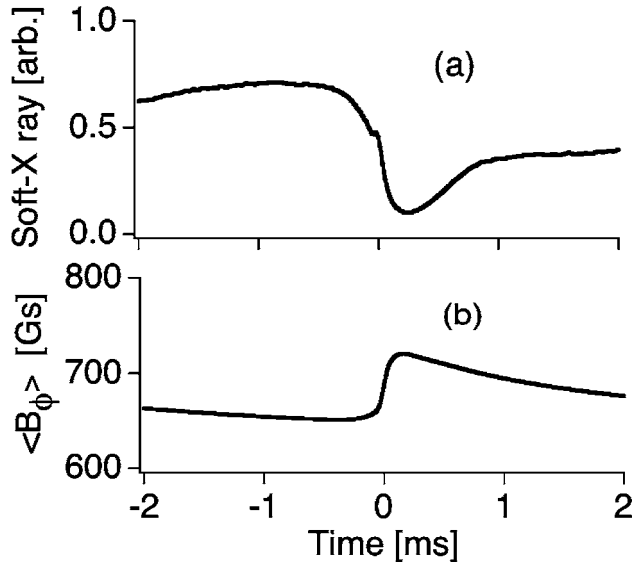
FIG. 2. Ensemble averaged sawtooth dynamics of (a) core plasma soft-x-ray emission and (b) average toroidal magnetic field during sawtooth cycle. Time $t=0$ denotes sawtooth crash.

FIG. 3. Dynamics of (a) equilibrium parallel current density profile and (b) inductive electric field over sawtooth crash.

ties over many reproducible sawtooth cycles, thereby eliminating the contribution of fluctuations. For example, ensemble averaged soft-x-ray emission over the sawtooth crash is plotted in Fig. 2(a), which indicates an electron temperature drop in the plasma core at the crash. Energy is suddenly released within approximately $100-200$ μs after the stable, slowly ramping ($2-3$ ms) heating phase. This cycle is very similar to sawtooth phenomena observed in tokamaks and other toroidal fusion devices. At the crash, one sees an increase in average toroidal magnetic flux as shown in Fig. 2(b) where $t=0$ denotes time of the crash. The prompt rise in $\langle B_\phi \rangle$ indicates that the RFP plasma itself must self-generate toroidal magnetic flux (dynamo effect) since there is no externally applied poloidal electric field. It should be noted that the total magnetic energy is reduced after a sawtooth crash even though the toroidal flux is increased.

Fast temporal dynamics of the parallel current density profile $J_\parallel(r,t)$ are determined by measuring magnetic field using Faraday rotation (for poloidal field), motional Stark effect (for toroidal field) and external magnetic coils.[18,20] As shown in Fig. 3(a), current density profile flattening during the sawtooth collapse requires very fast ($100-200$ μs) transport from the plasma core to the edge. This current transport timescale is much faster than a resistive time (~ 100 ms) for MST. The induced electric field near the magnetic axis associated with the sudden change of poloidal magnetic flux during relaxation is shown in Fig. 3(b). The force associated with $E_\parallel(r,t) \sim 40$ V/m is far greater than the collision force $\eta J \sim 1$ V/m. Moreover, although the enhanced electric field is in the same direction as the toroidal current density, $J_\phi(0)$ actually drops about 20% at the crash. Thus another force must be acting on the electrons to balance the electric field. Phenomenologically, one could attribute this effect to enhanced anomalous resistivity in the core. However, in the
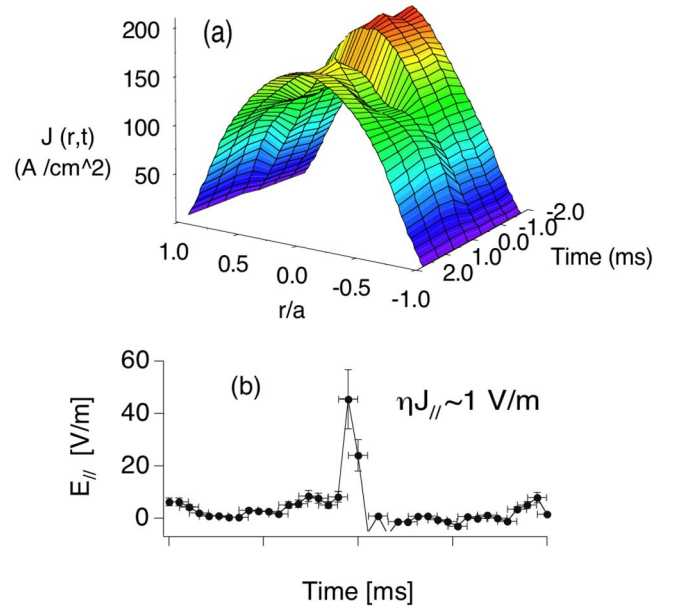
plasma edge the inductive electric field is perpendicular or even opposite to the current direction, making anomalous resistivity insufficient to balance the electric field. Therefore, a physical mechanism for the self-generation of current is required and needs to be experimentally identified. A magnetic fluctuation-induced electromotive force, either the MHD or Hall dynamo as shown in parallel Ohm's law [see Eq. (2)], is believed necessary to balance the electric field and redistribute the mean current during a relaxation event.

B. Parallel component of Hall dynamo

Before proceeding to describe measurements of the Hall dynamo effect in MST, it is necessary to first express the parallel component in a form most suitable for experimental determination. The poloidal and toroidal components in cylindrical coordinates are

$$\langle \delta J \times \delta B \rangle_\theta = \langle \delta j_\phi \delta b_r \rangle - \langle \delta j_r \delta b_\phi \rangle, \tag{7a}$$

$$\langle \delta J \times \delta B \rangle_\phi = \langle \delta j_r \delta b_\theta \rangle - \langle \delta j_\theta \delta b_r \rangle, \tag{7b}$$

where $\langle \cdots \rangle = (1/4\pi^2) \int_0^{2\pi} \int_0^{2\pi} d\theta d\phi$ denotes a magnetic surface average. These two components can be simplified by using $\nabla \cdot \delta \mathbf{B} = 0$, $\nabla \times \delta \mathbf{B} = \mu_0 \delta \mathbf{J}$, where $\langle i\delta b_l \delta b_l \rangle = 1/4\pi^2 \int_0^{2\pi} \int_0^{2\pi} i\delta b_l \delta b_l d\theta d\phi = 0$, $l=r,\theta,\phi$, $\partial/\partial\theta \to im$,, $\partial/\partial\phi \to in$ for a flux surface average. This yields

$$\mu_0 \langle \delta J \times \delta B \rangle_\theta = \mu_0 (\langle \delta j_\phi \delta b_r \rangle - \langle \delta j_r \delta b_\phi \rangle) = \left\langle \left(\frac{1}{r} \frac{\partial}{\partial r} r \delta b_\theta - \frac{1}{r} \frac{\partial}{\partial \theta} \delta b_r \right) \delta b_r \right\rangle - \left\langle \left(\frac{1}{r} \frac{\partial \delta b_\phi}{\partial \theta} - \frac{1}{R} \frac{\partial \delta b_\theta}{\partial \phi} \right) \delta b_\phi \right\rangle$$

$$= \left\langle \delta b_r \frac{1}{r} \frac{\partial}{\partial r} r \delta b_\theta \right\rangle - \left\langle -\frac{in}{R} \delta b_\theta \left(\frac{iR}{n} \frac{1}{r} \frac{\partial}{\partial r} (r \delta b_r) - \frac{R}{r} \frac{m}{n} \delta b_\theta \right) \right\rangle$$

$$= \left\langle \delta b_r \frac{1}{r} \frac{\partial}{\partial r} r \delta b_\theta \right\rangle - \left\langle \delta b_\theta \frac{1}{r} \frac{\partial}{\partial r} r \delta b_r \right\rangle. \tag{8a}$$

Similarly, we obtain

$$\mu_0 \langle \delta J \times \delta B \rangle_\phi = \mu_0 (\langle \delta j_r \delta b_\theta \rangle - \langle \delta j_\theta \delta b_r \rangle) = \left\langle \left(\frac{1}{r} \frac{\partial \delta b_\phi}{\partial \theta} - \frac{1}{R} \frac{\partial \delta b_\theta}{\partial \phi} \right) \delta b_\theta \right\rangle - \left\langle \left(\frac{1}{R} \frac{\partial \delta b_r}{\partial \phi} - \frac{\partial \delta b_\phi}{\partial r} \right) \delta b_r \right\rangle$$

$$= \frac{m}{r} \left\langle i \delta b_\theta \left[\frac{iR}{rn} \frac{\partial}{\partial r} (r \delta b_r) - R \frac{m}{rn} \delta b_\theta \right] \right\rangle + \left\langle \delta b_r \frac{1}{r} \frac{\partial (r \delta b_\phi)}{\partial r} \right\rangle$$

$$= -\frac{R}{r} \frac{m}{n} \left\langle \delta b_\theta \frac{1}{r} \frac{\partial}{\partial r} (r \delta b_r) \right\rangle + \left\langle \frac{1}{r} \frac{\partial}{\partial r} \left[\frac{iR}{n} \frac{\partial}{\partial r} (r \delta b_r) - R \frac{m}{n} \delta b_\theta \right] \delta b_r \right\rangle$$

$$= -\frac{R}{r} \frac{m}{n} \left\langle \delta b_r \frac{\partial}{\partial r} (\delta b_\theta) \right\rangle - \frac{R}{r} \frac{m}{n} \left\langle \delta b_\theta \frac{1}{r} \frac{\partial}{\partial r} (r \delta b_r) \right\rangle. \tag{8b}$$

The parallel component of Hall dynamo is defined as

$$\frac{\langle \delta \mathbf{J} \times \delta \mathbf{B} \rangle_\parallel}{n_e e} = \frac{\langle \delta \mathbf{J} \times \delta \mathbf{B} \rangle}{n_e e} \cdot \frac{\mathbf{B}}{B}$$

$$= \frac{1}{n_e e} \left[\langle \delta \mathbf{J} \times \delta \mathbf{B} \rangle_\theta \frac{B_\theta}{B} + \langle \delta \mathbf{J} \times \delta \mathbf{B} \rangle_\phi \frac{B_\phi}{B} \right]. \tag{9}$$

This expression can be further simplified in terms of $(\delta b_r, \delta b_\theta)$ in the vicinity of the resonant surface $(r = r_s)$ by using the relation $\mathbf{k} \cdot \mathbf{B} = (m/r_s) B_\theta + (n/R) B_\phi = 0$, leading to

$$\frac{\langle \delta \mathbf{J} \times \delta \mathbf{B} \rangle_\parallel}{n_e e} = \frac{A_1}{n_e e} \left\langle \delta b_r \frac{\partial}{\partial r} \delta b_\theta \right\rangle - \frac{A_2}{n_e e} \left\langle \frac{1}{r} \delta b_\theta \frac{\partial}{\partial r} r \delta b_r \right\rangle$$

$$+ \frac{B_\phi}{B} \frac{\delta b_r \delta b_\theta}{r} \frac{1}{n_e e} \approx A_1 \frac{\langle \delta j_\phi \delta b_r \rangle}{n_e e}, \tag{10}$$

where

$$A_1 = \frac{B_\theta}{B} \left[1 + \left(\frac{mR}{nr_s} \right)^2 \right] = \frac{B_\theta}{B} \left[1 + \left(\frac{B_\phi}{B_\theta} \right)^2 \right],$$

$$A_2 = \frac{B_\theta}{B} \left[1 - \left(\frac{mR}{nr_s} \right)^2 \right] = \frac{B_\theta}{B} \left[1 - \left(\frac{B_\phi}{B_\theta} \right)^2 \right].$$

B_ϕ, B_θ, and B are the known equilibrium toroidal, poloidal, and total magnetic field. The term

$$\frac{A_2}{n_e e} \left\langle \frac{1}{r} \delta b_\theta \frac{\partial}{\partial r} r \delta b_r \right\rangle$$

is found to be small in experiments (as will be shown later in Sec. III C) where $\delta b_\theta(r_s) \sim 0$ and $\partial \delta b_r / \partial r \ll \partial \delta b_\theta / \partial r$ for tearing modes. In addition,

$$\left(\frac{B_\phi}{B} \frac{\delta b_r \delta b_\theta}{r} \frac{1}{n_e e} \right) \le \frac{A_1}{n_e e} \left(\delta b_r \frac{\partial}{\partial r} \delta b_\theta \right)$$

near the resonant surface [see Eq. (10)]. To see this, we perform a Taylor expansion near resonant surface giving

$$\frac{\delta b_r \delta b_\theta}{r_s} = \delta b_r \left(\frac{\partial}{\partial r} \delta b_\theta \right) \left(\frac{r - r_s}{r_s} \right) \left(\delta b_r \frac{\partial}{\partial r} \delta b_\theta \right),$$

where

$$\left| \frac{r - r_s}{r_s} \right| < 1$$

and $\delta b_\theta(r_s) = 0$. Therefore, $A_1 \langle \delta j_\phi \delta b_r \rangle / n_e e$ is the dominant term in Eq. (10) and is used to determine the Hall dynamo near the resonant surface.

C. Hall dynamo measurement

To investigate the role of the Hall dynamo ($\langle \delta \mathbf{J} \times \delta \mathbf{B} \rangle_\parallel / n_e e$) on the mean current density profile, we require measurement of (1) the local current density fluctuation δj_ϕ; (2) local magnetic field fluctuations δb_r and δb_θ; and (3) their coherent interaction or correlation. In the following, each of these measurements will be discussed.

First, local current density fluctuations are measured directly by Faraday rotation. It has previously been established[22] that the current fluctuation between polarimeter chords can be described by

$$\delta I_\phi \approx \int_{x_1} \delta \mathbf{B} \cdot d\mathbf{l} - \int_{x_2} \delta \mathbf{B} \cdot d\mathbf{l} = \Delta \tilde{\psi} / c_F \bar{n}_e \mu_0, \tag{11}$$

where $\tilde{\psi} = c_F \int n_e \delta \mathbf{B} \cdot d\mathbf{l} \approx c_F \bar{n}_e \int \delta \mathbf{B} \cdot d\mathbf{l}$ is the fluctuating Faraday rotation signal, x_1 and x_2 are impact parameters of the selected chord pair, and $\bar{n}_e$ is the mean electron density.
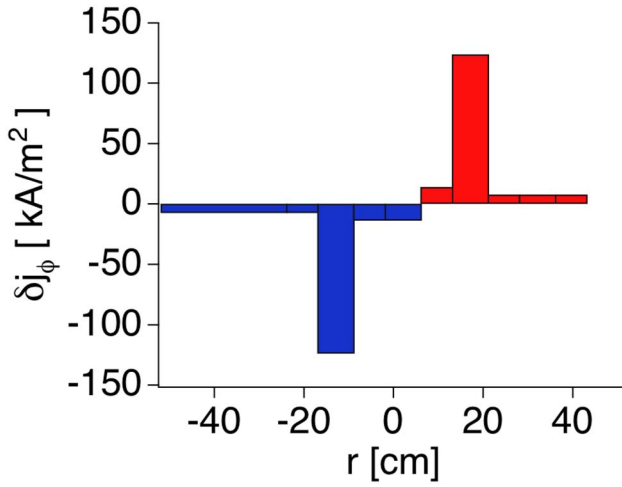
FIG. 4. Current density fluctuation spatial profile for (1,6) mode. Fluctuations peak at resonant surface and reverse sign cross magnetic axis.
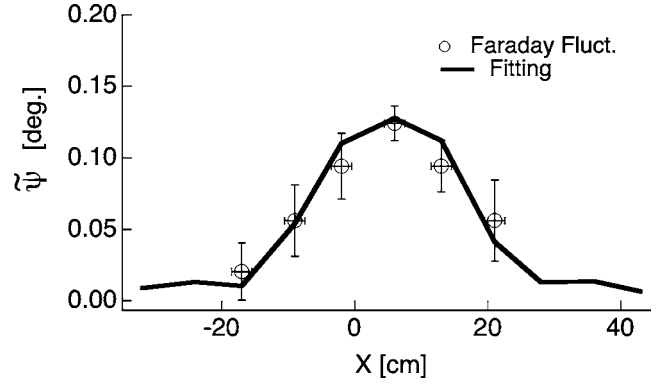

FIG. 5. Faraday rotation fluctuation amplitude for different chords. Circles represent measured Faraday rotation fluctuation. Solid line is fitting result.

Treating the density as constant and removing it from the integral is valid for MST profiles that are rather flat.[23] Errors introduced by this assumption are <10%. The above equation then represents a straightforward application of Ampère's law to the loop defined by adjacent Faraday rotation chords and holds true for the central six polarimeter chords where the density fluctuations are negligible due to the small density gradient in the core and the $m=1$ nature of the perturbation, as discussed earlier. This line-averaged measure of the current fluctuation (δI) can then be inverted to obtain the local current density perturbation $\delta j_\phi(r)$, through application of an asymmetric Abel inversion technique.[24] Since the measured helical current fluctuation is localized near the resonant surface, the local current density fluctuation δj_ϕ can be directly measured by the pair of chords nearest the resonant surface, as shown in Fig. 4. It is determined that the current density fluctuation (1) peaks at the resonant surface, (2) reaches an amplitude $\delta j_\phi/J_0 \sim 5\%$ -6% at the sawtooth crash, and (3) perturbation radial extension ≤ 8 cm. Results shown are for the dominant, core resonant, (1,6) tearing mode. Current density fluctuation dynamics are directly measured, thereby permitting one to correlate local current fluctuations to global magnetic fluctuations.

Second, the local magnetic fluctuation profile can be obtained by integrating the current fluctuation distribution. However, to determine more precisely the magnetic and current density fluctuation profiles, we have developed a simple fitting routine where it is assumed that the resonant current density fluctuation profile has the form $\delta j_\phi(r) = j_a \exp\{-[(r-r_s)/w]^2\}$, with j_a (amplitude), r_s (surface location), and w (width) serving as free parameters. Each parameter is quantified by making a best fit to the measured fluctuating Faraday rotation profiles. Once the fluctuating current density distribution is identified, the magnetic fluctuation spatial profile can be obtained by using $\nabla \times \delta B = \mu_0 \delta J$, $\nabla \cdot \delta B = 0$, and $\nabla \cdot \delta J = 0$ in a cylindrical geometry. Determination of the magnetic fluctuation spatial profile for a specific mode (m,n), is accomplished by integrating the above

equations assuming $\delta j_\perp \ll \delta j_\parallel$ and using the boundary condition $\delta b_r(a) = 0$. Therefore, a modeled Faraday rotation fluctuation for a specified current perturbation is described by

$$\tilde{\psi}^M(j_a, r_s, w) = c_F \int n_e(r)(\delta b_r \sin\theta + \delta b_\theta \cos\theta)dz$$

and can be constructed for each chord by minimizing

$$\chi^2 = \sum_{i=1}^{6} \frac{[\tilde{\psi}_i - \tilde{\psi}_i^M(j_a, r_s, w)]^2}{\sigma_i^2} + \frac{[\delta b_\theta^M(a) - b_\theta(a)]^2}{\sigma^2}$$

with respect to the free parameters (j_a, r_s, and w). For this expression, σ_i and σ are measurement errors, $b_\theta(a)$ is measured by magnetic coils mounted inside the vessel, and $b_\theta^M(a)$ is a modeled value. In the minimization procedure we specify j_a, r_s, and w and obtain both the magnetic field and current density fluctuation profiles. The measured Faraday rotation fluctuation profile and best fit result are shown in Fig. 5. Details of the analysis procedure have been previously described.[24]

The resulting magnetic field and current density fluctuation spatial profiles for the core resonant (1,6) mode are shown in Fig. 6. Uncertainty due to the fitting procedure and experimental error is also estimated. Radial magnetic field fluctuations are observed to extend continuously through the rational surface indicating their resistive nature. Poloidal
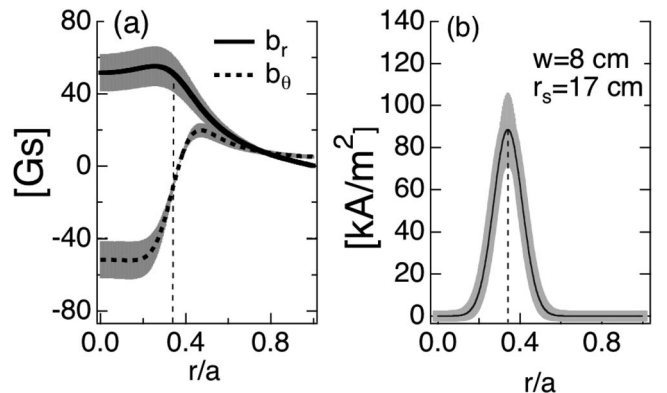

FIG. 6. (a) Radial and poloidal magnetic fluctuation spatial profile for dominant (1,6) mode. (b) Corresponding current density fluctuation spatial profile.
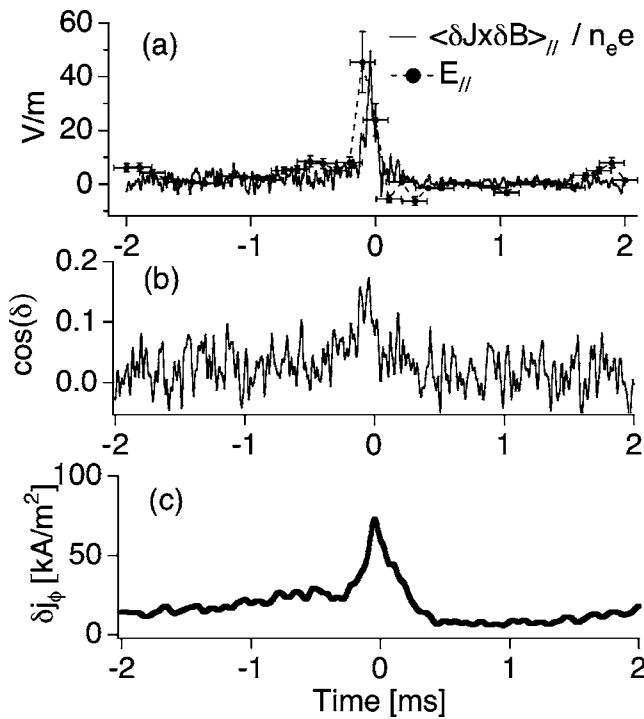
FIG. 7. (a) Dynamics of Hall dynamo (solid line) and inductive electric field (dashed line) during magnetic relaxation event. Time $t=0$ denotes the sawtooth crash. Data have been ensemble averaged over 380 independent sawtooth events. (b) Phase difference between current and magnetic field fluctuations and (c) current density fluctuations dynamics over sawtooth crash.

FIG. 8. Hall dynamo spatial profile for (1,6) mode showing a peak at the resonant surface.

magnetic fluctuations change sign across the resonant surface, in qualitative agreement with previous measurements by probes in OHTE and ZT-40[25] and MHD computation.[2,9] A maximum in the current density fluctuation ($\delta j_\phi/J_0 \sim 4.5\%$) occurs at $r_s=17$ cm where the (1,6) mode resonant surface is located based on equilibrium magnetic field measurements. The fluctuating current channel radial width is approximately 8 ± 3 cm. Amplitude, radial width, and location are all consistent with the direct current density fluctuation measurement discussed earlier in this section. Near the resonant surface, measurements show $\delta b_\theta(r_s) \sim 0$, $\partial b_r/\partial r \ll l\,\partial b_\theta/\partial r$, and $B_\phi \gtrsim B_\theta$, justifying the simplification made in Eq. (10), where the Hall dynamo parallel component was derived.

The current sheet width is greater than the resistive MHD layer (~ 0.2 cm) and ion acoustic gyroradius $\rho_s = 2.0$ cm. However, it is found to be comparable to the magnetic island width, and ion skin depth, $c/\omega_{pi} \sim 10$ cm in MST. Although the reconnection current layer width exceeds the simple linear MHD estimate, measured profiles are consistent with the tearing mode expectation that the current perturbation is local and magnetic perturbation is global.

Finally, the phase between δj_ϕ and δb_r can be obtained by ensemble averaging. In MST, rotation of the low-n magnetic modes transfers their spatial structure in the plasma frame into a temporal evolution in the laboratory frame. Since the magnetic modes are global, for convenience we correlate δj_ϕ to a specific helical magnetic mode obtained from spatial Fourier decomposition of measurements from 64 wall-mounted magnetic coils. After averaging over an ensemble of similar events, we can directly determine the phase
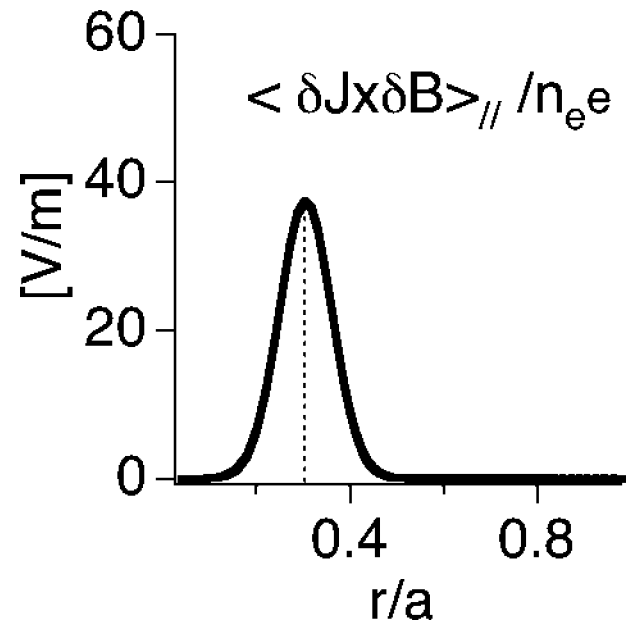
between $\delta j_\phi(r_s)$ and $\delta b_\theta(a)$ for the specified mode. Since (1) $\delta b_r(a)$ and $\delta b_\theta(a)$ have a fixed phase difference of $\pi/2$ at the edge where $j_r=0$ and (2) the radial magnetic perturbation is expected to have a constant phase at all radii for tearing modes[2,12] (which has been verified by probe measurements in lower temperature plasmas), we are able to determine the phase between $\delta j_\phi(r_s)$ and $\delta b_r(r_s)$. Using this information, along with the magnitude of $\delta b_r(r_s)$ from Fig. 6, we now evaluate $\langle \delta j_\phi(r_s)\delta b_r \rangle$ to determine the Hall effect.

The two-fluid Hall effect is measured to be nonzero with strong temporal dynamics. As shown in Fig. 7(a), the Hall dynamo begins increasing dramatically immediately prior to the sawtooth crash, reaching $\sim 50 \pm 10$ V/m, as shown by the solid line. This occurs because the phase difference between the fluctuating current and magnetic field deviates from 90° (by $\sim 10°$) and the current density (as well as magnetic field) fluctuations increase, as shown in Figs. 7(b) and 7(c). Away from the sawtooth crash, the Hall electric field (averaged over time window -2 to -1 ms) is relatively small. At this time, the current density fluctuation has a near 90° phase difference with radial magnetic field fluctuation, making the cosine of the phase small. The change in phase during the sawtooth crash is primarily ascribed to nonlinear mode coupling as will be discussed in Sec. III D.

The fluctuating current δj_ϕ peaks at the resonant surface and hence the Hall dynamo has a maximum there as well. As shown in Fig. 8, the measured width is ~ 8 cm. This is estimated by using Eq. (10) and assuming the current fluctuation phase is spatially constant. The estimated width of the Hall dynamo is subject to fairly large uncertainties (± 3 cm), since Eq. (10) is only valid near the resonant surface. Nevertheless, the Hall dynamo is maximum at the resonant surface and an additional dynamo mechanism may be required to balance the induced electric field elsewhere. This is especially true in the core where the spacing between adjacent low order ratio-

nal surfaces is largest. Such a picture is qualitatively consistent with quasilinear theory[12] which predicts a localized Hall dynamo and a more diffuse MHD dynamo away from the resonant surface. However, the measured Hall dynamo width is much greater than that predicted, even when taking the measurement uncertainty into account. These results imply that nonlinear dynamics play an important role.

The Hall dynamo effect is only measured in one location ($r/a=0.35$) corresponding to the (1,6) mode resonant surface. Contributions from other modes [i.e., (1,7), (1,8), …] to Hall dynamo at this location is negligible because current density fluctuations from these modes are measured to be small at $r/a=0.35$. The Hall dynamo in the core is found to oppose the mean current. From Fig. 7, it is observed that the large Hall electromotive force is comparable to the induced electric field (dashed line) and acts to suppress equilibrium current during plasma relaxation. The resistive force ηJ is small compared to both the induced electric field and the Hall dynamo during the sawtooth crash. This direct measurement of a substantial Hall dynamo in a high-temperature plasma indicates that two-fluid effects are necessary to understand plasma relaxation.

D. Nonlinear mode-mode interaction

For the Hall dynamo to be nonzero, the phase between the current density and magnetic field fluctuations for a contributing mode must differ from $\pi/2$. In MST, we observe that the phase deviates significantly from $\pi/2$ only when three-wave coupling is strong. That is, it appears that the phase between current and magnetic field for a specific mode is altered if that mode is nonlinearly coupled to other modes, and the alteration is such as to strengthen the Hall dynamo. We draw this conclusion by comparing the Hall dynamo in standard RFP plasmas to plasmas in which the dominant three-wave interactions are eliminated. This effect of nonlinear mode coupling is similar to recent results from MHD computation.[9]

Experimentally observed phase deviation from $\pi/2$ [see Fig. 7(b)] during a sawtooth crash implies that the Hall dynamo is enhanced. The phase change most likely originates from nonlinear mode coupling in MST plasmas since magnetic fluctuations can interact with the eddy currents generated by global magnetic field perturbations, similar to the effect of an error field[26] or imposed boundary.[27] The measured safety factor at the magnetic axis is $q(0)\sim0.2$, monotonically decreasing at large minor radii. It passes through zero at the reversal surface, being negative at the edge, as shown in Fig. 9. From the measured q profile, resonant low-n ($n=6$ is the resonant mode closest to the magnetic axis), $m=1$ magnetic modes will dominate the core magnetic fluctuation wave number spectrum as is frequently observed. In addition to the core resonant modes, $m=0$ ($n=1,2,…$) modes are resonant at the reversal surface. Both the $m=1$ and $m=0$ tearing modes have a global nature so that nonlinear mode coupling is common.[28–30] The three-wave interaction has to satisfy the sum rule
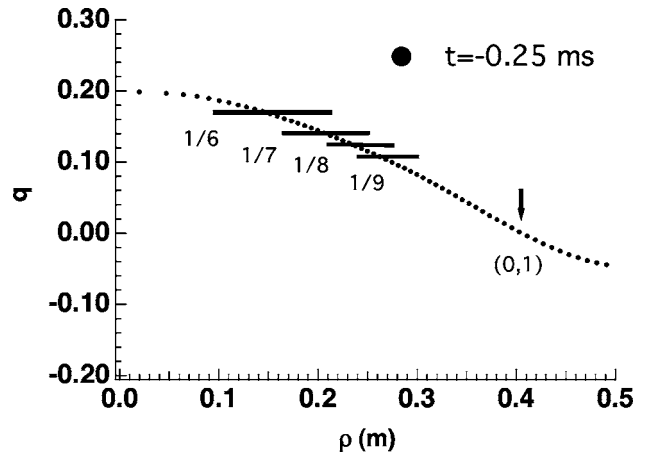

FIG. 9. The safety factor q profile 0.25 ms before sawtooth crash. The $m=1$ resonant surfaces and island width are indicated by solid line and the $m=0$ surface by arrow. Solid circles represent the measured q profile. Mode resonant surfaces are densely packed resulting in strong mode-mode interaction.

$$m_1 \pm m_2 = m_3 \quad \text{and} \quad n_1 \pm n_2 = n_3. \quad (12)$$

The coupling of two adjacent $m=1$ modes via interaction with an $m=0$ mode has been shown to be very important in both experiments and MHD computation.

A typical strong three-wave interaction observed in MST plasmas is that between the (1,6), (1,7), and (0,1) modes. The suppression of one mode is expected to result in a dramatic reduction in the nonlinear mode coupling. In order to identify the role played by nonlinear coupling in the Hall dynamo during the sawtooth crash, we compare standard RFP plasmas with those where the reversal surface (and the $q=0$ resonance surface) has been removed (i.e., nonreversed MST plasmas where the reversal surface is moved beyond or located at $r=a$). For reversed plasmas, the $m=1$, $n=5,6,7,…$ mode amplitudes during the sawtooth cycle are shown in Fig. 10(a), and found to be comparable to the nonreversed case, as shown in Fig. 10(b). This indicates that the $m=1$ mode does not decrease significantly for non-reversed plasmas. However, the $m=0$ mode amplitude is significantly reduced [see Fig. 10(c)] since its resonant surface is removed. For nonreversed plasmas, measurements reveal the Hall dynamo effect is reduced fivefold compared to standard RFP plasmas and is observed to peak at <10 V/m, as shown in Fig. 11(a). The phase between the localized current density fluctuations and global magnetic fluctuation for the (1,6) mode is also altered as shown in Fig. 11(b). From these results it is apparent that to have the phase differ significantly from 90°, substantial $m=0$ activity is needed, implying that the change in (1,6) mode phase between δj_ϕ and δb_r occurs due to nonlinear coupling.

IV. DISCUSSION

The measured two-fluid Hall effect and the role it plays in the plasma relaxation process provide experimental evidence for a new dynamo mechanism as well as insight into magnetic reconnection in RFP plasmas. However, the dynamo picture for the RFP remains incomplete. In this section,
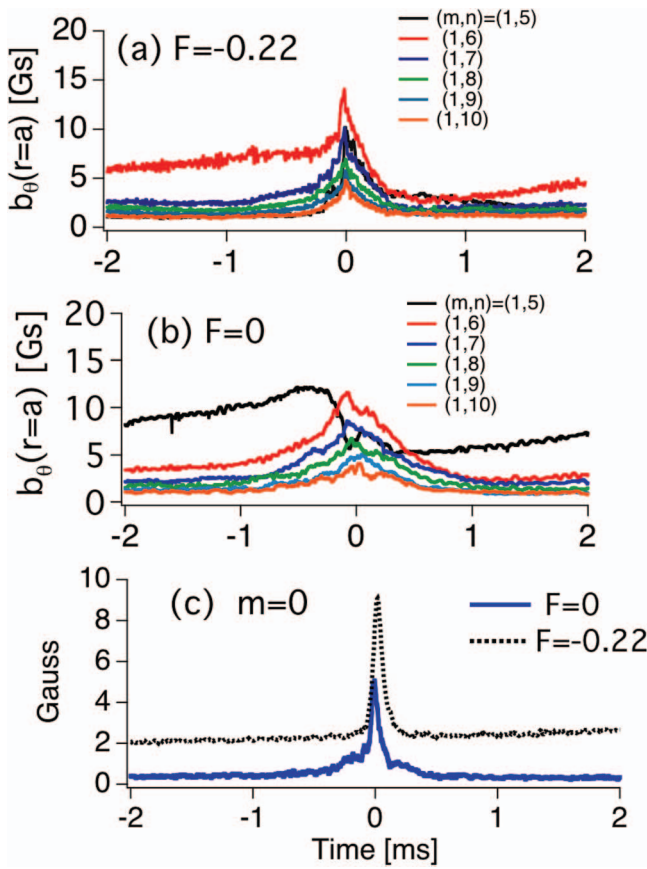
FIG. 10. (Color) Temporal dynamics of core resonant ($m=1$) modes over sawtooth cycle for (a) standard plasma ($F=-0.22$) and (b) nonreversed plasma ($F=0$); and (c) $m=0$ mode amplitude for standard ($F=-0.22$) and nonreversed ($F=0$) plasmas. Crash denoted by $t=0$.

we briefly discuss a few issues related to the Hall dynamo and MHD dynamo along with the role of Hall dynamo in magnetic reconnection.

A. Hall and MHD dynamos

In MST, the imbalance between inductive electric field and current exists over nearly the entire plasma column.[31] It is predicted that various dynamo mechanisms may be playing a role in providing the required balance. Both Hall dynamo and MHD dynamo have been identified experimentally in MST with the relative weighting of these two effects throughout the plasma cross section being a topic of great interest.

As mentioned in the Introduction, probes inserted at the plasma edge have measured a significant MHD dynamo for $r/a > 0.90$. The MHD dynamo is balanced by local electric field, consistent with RFP MHD computation.[9] However, at the innermost probe position ($r/a=0.85$), the effect is no longer observed.[10] Previous Hall dynamo measurements by magnetic probes show it to be relatively small in the edge region ($r/a=0.92$), contributing ~25% to total electric field, but becoming significant further inward at $r/a=0.85$.[15]

These measurements reveal a spatial trend opposite that of the MHD dynamo. In the plasma core, it is observed that the Hall dynamo dominates near the resonant surface for the
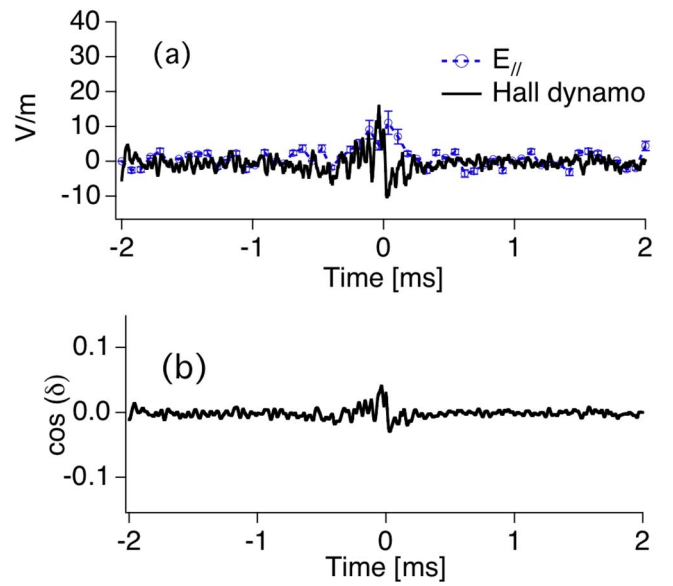

FIG. 11. (a) Hall dynamo and inducted electric field $E_\parallel$ and (b) phase between current and magnetic field fluctuations, for nonreversed ($F=0$), reduced $m=0$ mode plasmas.

(1,6) mode ($r/a=0.35$), as shown in Fig. 7. For this region the Hall dynamo alone is sufficient to balance the electric field, thereby implying the MHD dynamo is small. To date, Hall dynamo measurements have not been made in the region $0.5 \leq r/a \leq 0.8$, due to large density fluctuations which complicate extraction of magnetic field fluctuation information from the Faraday rotation measurements. Work in this area is actively being pursued. Based on measurements at the (1,6) mode resonant surface, it seems reasonable to expect that a similar Hall dynamo should occur at the (1,7), (1,8), (1,9), etc., resonant surfaces as well. Since these resonant surfaces become more closely spaced with increasing toroidal mode number (see Fig. 9), the Hall dynamo may essentially become quasicontinuous in this region. This may also hold true in the region $0.35 \leq r/a \leq 0.5$, where spacing between the (1,6) and (1,7) mode resonant surfaces is ~5 cm and comparable to the Hall dynamo width shown in Fig. 8. However, magnetic stochasticity may also be playing a role thereby pointing out the need for a direct measurement at other resonant surfaces. Previous line-averaged MHD dynamo measurements[11] by Doppler spectrometry indicate a nonzero MHD dynamo in the core but the spatial distribution remains unresolved.

An interesting question is whether the MHD dynamo plays any role at the resonant surface location where the Hall dynamo effect is maximum. An active MHD dynamo at the resonant surface requires a finite correlation between radial velocity fluctuations and magnetic fluctuations. To see this, we express the MHD dynamo parallel component at the resonant surface in cylindrical coordinates:

$$\langle \delta\mathbf{v} \times \delta\mathbf{B}\rangle_\parallel = \left(\langle\delta\mathbf{v}\times\delta\mathbf{B}\rangle_\theta \frac{B_\theta}{B} + \langle\delta\mathbf{v}\times\delta\mathbf{B}\rangle_\phi \frac{B_\phi}{B}\right), \quad (13)$$

where $\langle\delta\mathbf{v}\times\delta\mathbf{B}\rangle_\theta = \langle\delta v_\phi \delta b_r\rangle - \langle\delta v_r \delta b_\phi\rangle$, $\langle\delta\mathbf{v}\times\delta\mathbf{B}\rangle_\phi = \langle\delta v_r \delta b_\theta\rangle - \langle\delta v_\theta \delta b_r\rangle$. If δv_r does not correlate with magnetic fluctuations, Eq. (13) can be rewritten as

$$\langle \delta \mathbf{v} \times \delta \mathbf{B} \rangle_{\parallel} = \langle \delta v_\phi \delta b_r \rangle \frac{B_\theta}{B} - \langle \delta v_\theta \delta b_r \rangle \frac{B_\phi}{B}$$

$$= \frac{r}{m} \frac{1}{B} (\mathbf{k} \cdot \mathbf{B}) \langle \delta v_\phi \delta b_r \rangle, \tag{14}$$

where $\nabla \cdot \delta \mathbf{v} = 0$ is used. However, at the resonant surface, $\mathbf{k} \cdot \mathbf{B} = 0$ making the MHD dynamo vanish. Finite correlation between radial velocity fluctuations and magnetic fluctuations is therefore required for the MHD dynamo to be active at the resonant surface. To date, measurements have not observed a finite correlation between radial velocity fluctuations and magnetic fluctuations[11] implying $\langle \delta \mathbf{v} \times \delta \mathbf{B} \rangle_{\parallel}$ vanishes at the resonant surface. By combining measurements of Hall dynamo and MHD dynamo, both edge and core, a picture emerges where the Hall effect dominates in the vicinity of the resonant surface whereas the MHD dynamo may be active elsewhere. This experimental picture is similar to quasilinear theory[12] which shows the Hall dynamo dominating at the resonant surface where ions and electron are decoupled, but MHD dynamo active elsewhere.

New measurements of local ion velocity fluctuations by charge exchange recombination spectroscopy are being developed on MST to explore the detailed spatial profile of the MHD dynamo.[32] Meanwhile, electron velocity measurement by the relativistic Fizeau effect is also being developed on MST and potentially provides an electron dynamo measurement (combination of MHD and Hall dynamo) in the plasma core.[33]

B. Reconnection time in MST plasmas

The magnetic reconnection time for typical MST plasmas is about 100 μs. Sawtooth reconnection in the RFP shares many similar features with the tokamak. Fast reconnection occurs near a layer formed at the resonant surface and poloidal flux is removed during the reconnection process. Kadomtsev introduced a magnetic reconnection model for the tokamak sawtooth crash by considering finite resistivity effects during reconnection.[34,35] This is similar to the Sweet-Parker model,[4] where a collision term in parallel Ohm's law is included, giving

$$E + v_r B^* = \eta J, \tag{15}$$

where B^* is the helical component of the magnetic field. Later, Wesson[4] introduced an electron inertial term into Eq. (15) to explain fast reconnection for larger tokamaks. According to Ohm's law, the Kadomtsev reconnection time is

$$\tau_K \sim \sqrt{\tau_R \tau_A}, \tag{16}$$

where τ_R the is resistive time and τ_A is Alfvén time. For typical MST parameters, we find $\tau_A \sim 1$ μs, and $\tau_R \sim \mu_0 r_s^2 / \eta \sim 200$ ms. The computed $\tau_K \sim 450$ μs for MST plasmas is much slower than experimental observations (~ 100 μs). Based on results provided in this paper, this difference is not surprising since parallel Ohm's law near the resonant surface on MST is essentially balanced by the two-fluid Hall dynamo effect associated with nonlinear mode-mode coupling rather than a resistive collision term.

We can heuristically treat the Hall dynamo as an "anomalous" resistivity in Ohm's law [Eq. (15)] given by

$$\eta^* = \frac{\langle \delta \mathbf{J} \times \delta \mathbf{B} \rangle_{\parallel}}{ne} \frac{1}{J_{\parallel}}. \tag{17}$$

The time-averaged Hall dynamo amplitude during reconnection is about 20 V/m, and the equilibrium current density $J_{\parallel} \sim 2.2$ MA/m^2 leading to an anomalous resistive time $\tau^*_R \sim \mu_0 r_1^2 / \eta^* \sim 4.4$ ms, and an estimated reconnection time $\sqrt{\tau^*_R \tau_A} \sim 66$ μs. This result is faster than the Kadomtsev reconnection time and much closer to experimental observation. It should be pointed out that magnetic reconnection in MST is much more complicated in reality. Magnetic reconnection simultaneously occurs at different locations (i.e., different resonant surfaces) and the global interaction of magnetic reconnection events regulates the magnetic reconnection time. Proper treatment may require a fully nonlinear two-fluid MHD computation.

V. CONCLUSION

In summary, time-resolved observations of current density fluctuations and magnetic field fluctuations in a high-temperature collisionless plasma have been made by using a fast, laser-based, Faraday rotation diagnostic. The amplitude, temporal dynamics, spatial distribution, and phase relation between current density and magnetic fluctuations for the dominant, core resonant, (1,6) mode have been measured. These electromagnetic fluctuations have characteristics consistent with expectations for resistive tearing modes.

The Hall electromotive force along the mean magnetic field direction, $\langle \delta \mathbf{J} \times \delta \mathbf{B} \rangle_{\parallel} / n_e e$, is also determined and found to be significant near the mode resonant surface. The Hall dynamo acts to reduce mean current density in the core and balances the electric field induced at a sawtooth crash. Experiments demonstrate that nonlinear mode-mode coupling is an essential ingredient to generate a significant Hall dynamo. Nonlinear mode coupling alters the phase relation between the current density and magnetic field fluctuations with significant phase deviation from $\pi/2$ occurring only when three-wave coupling is strong. The Hall effect dominates in the vicinity of the resonant surface whereas the MHD dynamo may be active elsewhere.

ACKNOWLEDGMENTS

[1] J. Wesson, *Tokamaks* (Oxford University Press, New York, 1997).
[2] S. Ortolani and D. D. Schnack, *Magnetohydrodynamics of Plasma Relaxation* (World Scientific, Singapore, 1993).
[3] L. Spitzer, Jr., *Physics of Fully Ionized Gases*, 2nd ed. (Interscience, New York, 1962), p. 28.
[4] E. Priest and T. Forbes, *Magnetic Reconnection* (Cambridge University Press, New York, 2000).

[5]D. Biskamp and E. Scharz, Phys. Plasmas **8**, 4729 (2001).

[6]J. A. Wesson, Nucl. Fusion **30**, 2545 (1990).

[7]A. J. Lichtenberg, K. Itoh, S.-I. Itoh, and A. Fukuyama, Nucl. Fusion **32**, 495 (1992).

[8]R. N. Dexter, D. W. Kerst, T. W. Lovell, S. C. Prager, and J. C. Sprott, Fusion Technol. **19**, 131 (1991).

[9]E. J. Caramana, R. A. Nebel, and D. D. Schnack, Phys. Fluids **26**, 1305 (1983); Y. L. Ho and G. G. Graddock, Phys. Fluids B **3**, 721 (1991); A. Nagata *et al.*, Phys. Fluids B **3**, 1263 (1993).

[10]P. W. Fontana *et al.*, Phys. Rev. Lett. **85**, 566 (2000).

[11]D. J. Den Hartog, J. T. Chapman, D. Craig *et al.*, Phys. Plasmas **6**, 1813 (1999).

[12]V. V. Mirnov, C. C. Hegna, and S. C. Prager, Plasma Phys. Rep. **29**, 612 (2003).

[13]P. D. Mininni, D. O. Goemez, and S. M. Mahajan, Astrophys. J. **587**, 472 (2003).

[14]R. A. Nebel, *Proceeding of the Workshop on physics of Alternative Magnetic Confinement Schemes, Varenna, Italy, 15–24 October 1990* (Italy Physics Society, Bologna, 1991), p. 611.

[15]W. Shen and S. C. Prager, Phys. Fluids B **5**, 1931 (1993); A. F. Almagri, D. Craig, D. J. Den Hartog, G. Fiksel, V. Mirnov, S. C. Prager, and J. S. Sarff, Bulletin of the the 45th Annual Meeting of American Physical Society, 2003, Vol. 48, pp. 271.

[16]W. X. Ding, D. L. Brower, D. Craig, B. H. Deng, G. Fiksel, V. Mirnov, S. C. Prager, J. S. Sarff, and V. Svidzinski, Phys. Rev. Lett. **93**, 045002 (2004).

[17]D. L. Brower, W. X. Ding, S. D. Terry, J. K. Anderson, T. M. Biewer, B. E. Chapman, D. Craig, C. B. Forest, S. C. Prager, and J. S. Sarff, Rev. Sci. Instrum. **74**, 1534 (2003).

[18]D. L. Brower, W. X. Ding, S. D. Terry, J. K. Anderson, T. M. Biewer, B. E. Chapman, D. Craig, C. B. Forest, S. C. Prager, and J. S. Sarff, Phys. Rev. Lett. **88**, 185005 (2002).

[19]Y. Jiang, D. L. Brower, and L. Zeng, Rev. Sci. Instrum. **68**, 902 (1997).

[20]S. D. Terry, D. L. Brower, W. X. Ding, J. K. Anderson, T. M. Biewer, B. E. Chapman, D. Craig, C. B. Forest, S. C. Prager, and J. S. Sarff, Phys. Plasmas **11**, 1079 (2004).

[21]J. K. Anderson, T. M. Biewer, C. B. Forest, R. O'Connell, S. C. Prager, and J. S. Sarff, Phys. Plasmas **11**, L9 (2004).

[22]W. X. Ding, D. L. Brower, S. D. Terry, D. Craig, S. C. Prager, J. S. Sarff, and J. Wright, Phys. Rev. Lett. **90**, 035002 (2003).

[23]N. E. Lanier, D. Craig, J. K. Anderson *et al.*, Phys. Plasmas **8**, 3402 (2001).

[24]W. X. Ding, D. L. Brower, B. H. Deng, D. Craig, S. C. Prager, and V. Svidzinski, Rev. Sci. Instrum. **75**, 3387 (2004).

[25]R. J. La Haye *et al.*, Phys. Fluids **27**, 2576 (1984); G. Miller, *Proceeding of the Workshop on Physics of Alternative Magnetic Confinement Schemes, Varenna, Italy, 15–24 October 1990* (Italy Physics Society, Bologna, 1991), p. 257.

[26]R. Fitzpatrick, Nucl. Fusion **33**, 1049 (1993).

[27]X. G. Wang, Z. W. Ma, and A. Bhattacharjee, Phys. Plasmas **3**, 2129 (1996); Z. W. Ma, X. G. Wang, and A. Bhattacharjee, Phys. Plasmas **3**, 2427 (1996).

[28]A. K. Hansen, A. F. Almagri, D. Craig, D. J. Den Hartog, C. C. Hegna, S. C. Prager, and J. S. Sarff, Phys. Rev. Lett. **85**, 3408 (2000); S. Assadi, S. C. Stewart, and K. L. Sidikman, Phys. Rev. Lett. **69**, 281 (1992).

[29]R. G. Watt and R. A. Nebel, Phys. Fluids **26**, 1168 (1983).

[30]T. Bolzonella and D. Terranova, Plasma Phys. Controlled Fusion **44**, 2569 (2002).

[31]J. K. Anderson, J. Adney, A. Almagri *et al.*, Phys. Plasmas **12**, 056118 (2005).

[32]D. Craig, D. J. Den Hartog, G. Fiksel, V. I. Davydenko, and A. A. Ivanov, Rev. Sci. Instrum. **72**, 1008 (2001).

[33]D. L. Brower, W. X. Ding, B. H. Deng, M. A. Mahdavi, V. Mirnov, and S. C. Prager, Rev. Sci. Instrum. **75**, 3399 (2004).

[34]B. B. Kadomtev, Sov. J. Plasma Phys. **1**, 389 (1976).

[35]F. Porcelli, D. Boucher, and M. N. Rosenbluth, Plasma Phys. Controlled Fusion **38**, 2163 (1996).